Location Specific Temperature Compensation of Guided Wave Signals in Structural Health Monitoring

Stefano Mariani, Sebastian Heinlein, and Peter Cawley

***Abstract*— In guided wave structural health monitoring, defects are typically detected by identifying high residuals obtained through the baseline subtraction method, where an earlier measurement is subtracted from the "current" signal. Unfortunately, varying environmental and operational conditions (EOCs), such as temperature, also produce signal changes and hence, potentially, high residuals. While the majority of the temperature compensation methods that have been developed target the changed wave speed induced by varying temperature, a number of other effects are not addressed, such as the changes in attenuation, the relative amplitudes of different modes excited by the transducer, and the transducer frequency response. A temperature compensation procedure is developed, whose goal is to correct any spatially dependent signal change that is a systematic function of temperature. At each structural position, a calibration function that models the signal variation with temperature is computed and is used to correct the measurements, so that in the absence of a defect the residual is reduced to close to zero. This new method was applied to a set of guided wave signals collected in a blind trial of a guided wave pipe monitoring system using the T(0, 1) mode, yielding residuals de-coupled from temperature and reduced by at least 50% as compared with those obtained using the standard approach at positions away from structural features, and by more than 90% at features such as the pipe end. The method, therefore, promises a substantial improvement in the detectability of small defects, particularly at the existing pipe features.**

***Index Terms*— Baseline subtraction, defect detection, pipe inspection, temperature compensation.**

I. Introduction

INSPECTION systems based on guided waves are widely used to detect damage in structures found in numerous fields, such as aerospace, energy, and oil and gas. The main advantage of these systems over conventional ultrasonic techniques is their ability to inspect large areas of the structure from a single sensor location [1]. A well-established application is the testing of pipes for the oil and gas industry by means of the first-order torsional wave mode using a pulse-echo configuration at frequencies in the order of tens of kilohertz [2]. This wave mode offers a virtually uniform coverage of the entire pipe-wall and a very low attenuation in steel, thus enabling inspection for tens of meters from the sensor location [3]. The drawback is a reduced sensitivity to the changes in the pipe cross section, particularly when the guided wave sensors are used in a one-off inspection configuration. In this setting, the sensor is deployed on the structure and it is then removed after taking one or a few measurements. The sensor typically consists of two rings of transducers positioned roughly a quarter wavelength apart in the axial direction of the pipe to enable direction control [2]. The transducers, which can either be piezoelectric- or electromagnetic acoustic transducer (EMAT)-based, are evenly distributed around the ring and apply a tangential force to the pipe surface, hence exciting the torsional mode.

Unfortunately, in addition to the desired T(0, 1) torsional wave mode, other signal components exist due to imperfect direction control [2] and to the excitation and reception of unwanted modes. The latter is partly due to the finite number of transducers generating the tangential forces at discrete locations rather than uniformly around the external circumference of the pipe; this can result in the excitation of circumferential A0- and S0-like modes [4]. Theoretically, the generation of flexural modes can be prevented by ensuring that the number of elements in the ring is greater than k, where F(k, 1) is the highest order flexural mode whose cutoff frequency is within the bandwidth of the excitation signal [5]. However, in practical systems, some nonuniform transduction sensitivity of the transducers around the circumference is inevitable and will break the desired axisymmetry, hence generating (and receiving) flexural modes and enhancing the amplitude of the circumferential modes [6].

Because these unwanted signal components are deterministic, they cannot be eliminated through averaging, and hence they set a background noise level which is referred to as coherent noise. Defects must produce a reflection somewhat larger than this noise for reliable detection in a one-off inspection [6]. For this reason, the defect "call level" is typically set to reflection amplitudes corresponding to anomalies (e.g., defects) that present approximately 5% change in the cross-sectional area (CSA) of the pipe [7]. This value can

Manuscript received June 17, 2019; accepted August 8, 2019. Date of publication September 6, 2019; date of current version December 26, 2019. This work was supported by Guided Ultrasonics Ltd., and the Engineering and Physical Sciences Research Council (EPSRC) through the U.K. Research Centre in Non-Destructive Evaluation (RCNDE) under Grant EP/L022125/1. The work of S. Heinlein was supported by EPSRC and RCNDE through the Engineering Doctorate Studentship under Grant EP/I017704/1. *(Corresponding author: Stefano Mariani.)*

S. Mariani and P. Cawley are with the Department of Mechanical Engineering, Imperial College London, London SW7 2AZ, U.K. (e-mail: s.mariani@imperial.ac.uk; p.cawley@imperial.ac.uk).

S. Heinlein was with the Department of Mechanical Engineering, Imperial College London, London SW7 2AZ, U.K. He is now with Guided Ultrasonics Ltd., Brentford TW8 8HQ, U.K. (e-mail: sebastian.heinlein@guided-ultrasonics.com).

Digital Object Identifier 10.1109/TUFFC.2019.2940451

vary significantly depending on the general condition of the inspected pipe, the position of the defect, and the presence of other pipe features, such as welds, that also give reflections [8].

Recently, there has been a strong interest in moving from the standard one-off inspection configuration to a permanently installed monitoring system (PIMS), which is particularly appealing when dealing with cases of high access costs (e.g., pipes buried underground), and allows for frequent collection and interpretation of data [8]. The frequent monitoring potentially allows for the detection of damage at earlier stages, and the advantages of the PIMS over the one-off inspection systems are expected to be even greater for defects occurring in the vicinity of structural features that generate reflections even in the absence of defects. A further benefit enabled by the use of PIMS is that after a positive detection, the progression of damage can easily be monitored so that predictions on the remaining life of the structure can be attempted. Recent publications presented examples of such systems based on piezoelectric transducers [9], [10], Lorentz-force-based EMAT transducers [11], and magnetostrictive-based EMATs [12].

In a PIMS setting, the data analysis typically involves comparing new measurements with the baseline records, where any change in signals could represent a defect signature. Alongside the conventional baseline subtraction method [13], recently some authors have proposed detection procedures based on the signal decomposition methods, such as singular value decomposition (SVD) [14] and independent component analysis (ICA) [15]–[17]. Unfortunately, most of these methods are hindered by the effects of changing environmental and operational conditions (EOCs), primarily temperature [18]–[20], which are also responsible for the changes in the signals, hence degrading the damage detection performance. A possible solution to the problem, tailored for the baseline subtraction method, would be the early collection of a large number of baselines acquired under different EOCs, followed by a selection of the best one to be subtracted from any later reading, in a procedure called optimal baseline selection (OBS) [21], [22]. However, such a solution is often impractical as a very large number of baseline signals are required at small increments of the operating condition [20].

Focusing on the effects of temperature variations, a well-studied phenomenon is the induced change in the velocity of the guided wave modes [18]. To compensate for this effect, a technique called baseline signal stretch (BSS) was proposed in [20], [21], and [23]. The idea is to compress or dilate each signal by some stretch factor that minimizes the residuals between the signal itself and a baseline measurement. This process captures the physics of the effect of temperature changes well except that the process of time-stretching slightly distorts the frequency content of the signal, an effect that is termed "frequency noise" [24]. Recently, Harley and Moura [25] proposed a new computationally fast algorithm to perform BSS making use of the scale transform domain.

However, there are other, less-studied, effects caused by temperature variations on the wave propagation. First, referring to the systems using piezoelectric sensors, when the temperature changes, the bonding stiffness at the interface between each transducer and the structure is likely to vary, leading to frequency response changes that can affect both the amplitude and the phase of the signal [20], [26], [27]. In addition, if the system is operated close to resonance, a ringing effect may be observed at some temperatures. Similar phenomena are also seen with the EMAT-based systems [11], [28], where the transduction sensitivity is affected by circumferential variations in the permeability of the pipe [29]. Furthermore, as the wave velocity changes with temperature, so does the wavelength, thus varying the efficacy of the direction control, which relies on the spacing between the two rings of transducers being a known fraction of the wavelength [2]. Finally, some applications of the guided-wave-based monitoring systems are affected by strong signal attenuation, which is usually temperature dependent, for example, monitoring of a pipe coated with a viscoelastic material such as bitumen. Recently, Mariani *et al.* [6] proposed a phase compensation procedure that concurrently targets wave speed and transducer phase response changes. In this article, this will be denoted as the phase and stretch compensation (PSC) procedure.

Importantly, any change to the balance of transduction around the pipe or to the transducer frequency responses is likely to alter the generation of unwanted flexural and circumferential modes, and hence modify the coherent noise in a way that is not corrected by previous temperature compensation methods. Specifically, at each temperature, the unique balance of excited unwanted modes which travel at different velocities, the velocities being in general a function of frequency (i.e., the modes are dispersive), will give constructive and destructive interference at different positions along the pipe, so that the coherent noise is a spatially dependent function of temperature. For example, let us suppose that the monitoring system generates both the F(1, 2) and F(2, 2) modes in different ratios at different temperatures. Because their velocities are different, the sum of their amplitudes is a function of position and temperature; the same phenomenon also affects the sum of the A0- and S0-like circumferential modes at different positions. Similarly, the coherent noise caused by imperfect direction control is also a spatially dependent function of temperature, and the noise at a given location and temperature will also be a function of the attenuation of the different modes.

Therefore, because the coherent noise is a function of both temperature and location along the pipe, it cannot be perfectly compensated by a "global" compensation method such as the BSS or PSC methods developed previously (which involve modifying the whole signal using only one or two "global" parameters), and further, axial-location-dependent, compensation is required, where each axial location corresponds to one sample of the received signal. Because the transduction and attenuation changes causing the variation in coherent noise are expected to be a function of temperature that does not vary with time, a calibration function defining the variation in noise with the temperature at each axial location can be computed and used to correct the measurements. This is the essence of a novel procedure that will be called the location-specific temperature compensation (LSTC) method and that is presented in this article. Importantly, for its application, there is no requirement for any prior knowledge of the exact source of noise at each temperature (i.e., which exact combination

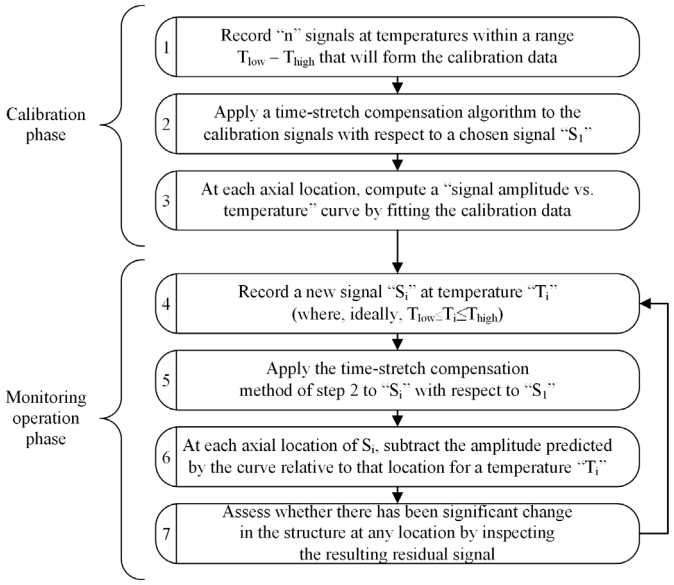

Fig. 1. Flowchart description of the LSTC method for assessing the integrity of a structure.

of unwanted modes is present), which greatly simplifies the problem. This new method was applied to a guided wave PIMS using the T(0, 1) wave mode. As will be shown, the final goal of the method is to minimize the residual obtained at each pipe location by comparing a set of early measurements taken over a range of temperatures with any later reading acquired on the structure, so that in the absence of a defect, the residual will be close to zero, making it easier to detect the presence of any signal changes produced by a defect.

This article is structured as follows. The proposed temperature compensation method is presented in Section II. Section III compares the results of the new method with those obtained with the conventional baseline subtraction method on an experimental data set. In particular, Section III-A quantifies the improvement brought by the new technique in a single test, while Section III-B shows the added benefits of analyzing trends of residuals across a number of measurements collected over time. The capability of compensating for temperature-dependent attenuation of guided wave signals is illustrated in Section III-C using synthetically modified experimental signals. It is then demonstrated in Section III-D how the new method can also be applied to the weights produced by ICA applied on the data set. Section IV gives the main conclusions of the study.

II. Location Specific Temperature Compensation Method

The LSTC method comprises two phases, namely, a calibration phase (steps 1–3) and a monitoring operation phase (steps 4–7), as shown in Fig. 1. In the calibration phase, the guided wave instrumentation acquires n signals at different temperatures within a temperature range "T_{low}–T_{high}" (step 1), which will form the calibration data for the LSTC. The number n of measurements needs to be sufficient to define the function of temperature; this is expected to be smoothly varying, so a modest number of measurements distributed over the temperature range of interest is sufficient. A signal (e.g., the first available one, here denoted "S_1") is chosen as the signal to which all subsequent measurements will be compared for the compensation of the temperature-dependent T(0, 1) wave speed, which can be accomplished using either the PSC procedure or the standard BSS method (step 2). The next step is the computation of a "signal amplitude versus temperature" calibration curve for each axial location (i.e., each sample of the received signals) (step 3). This is achieved by fitting the set of the RF signal amplitudes obtained at each axial location in the measurements forming the calibration data with an appropriate curve; order 4 polynomial fits were used in the results presented here.

In the monitoring operation phase, the guided wave instrumentation acquires a new waveform "S_i" at some temperature "T_i" (step 4), which is first compensated for the temperature-dependent wave speed (step 5, the same as step 2). Ideally, the temperature "T_i" would lie in the range $T_{low} \leq T_i \leq T_{high}$. For "$T_i$" outside the calibration temperature range, the accuracy of the compensation procedure would depend on the accuracy of extrapolation of the fitting curves out of the range. At each axial location of "S_i," the value predicted by the curve computed for that location and for a temperature equal to "T_i" is subtracted from the current measured value at the given location (step 6). It is worth noting that the calibration curves will have negative values for the RF values with a negative sign, but this does not alter the procedure. The result of this process is a newly formed residual signal, which can be interrogated to check whether there has been a significant change in the structure at any location (step 7). In operation, each successive acquired signal is compensated according to steps 4–7 and any significant change at any location is identified.

The description above implicitly assumes that the structure is defect-free before the acquisition of the calibration signals and that defects do not grow in the period of calibration data acquisition. However, if a defect is already present before the acquisition of the calibration waveforms, while the method would not be able to give any indication of the preexisting defect, it would still be able to detect later damage growth; if defect growth were to occur during the calibration phase, the calibration would be less accurate. If direct temperature readings are not available, the entire procedure can be performed using an indirect temperature measurement such as the time of arrival of a reflector or the stretch factor computed by the BSS method. The latter has the advantage that the operator does not need to know *a priori* about the existence or the location of reflectors in the structure.

III. Application of LSTC to Experimental Data

The new LSTC method described above was applied to a data set of ultrasonic-guided wave signals acquired by a Guided Ultrasonics Ltd. gPIMS sensor ring [30] set to use the T(0, 1) wave mode. The sensor ring was attached to an 8-in schedule 40 pipe whose layout is shown in Fig. 2 and which was installed in a temperature-controlled laboratory setting [9]. The excitation was an eight-cycle toneburst centered at 25.5 kHz. The pipe comprised 7- and 2-m straight sections connected by a 90° elbow (with a bend radius of 1.5 times the

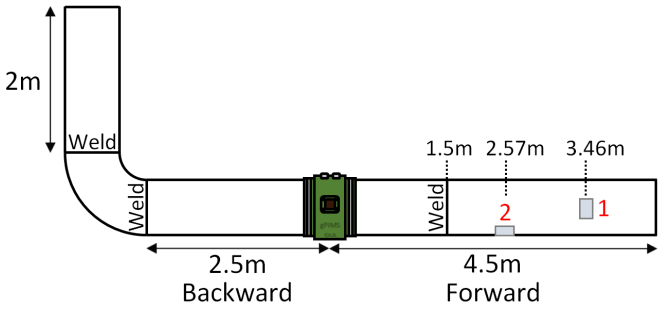

Fig. 2. Geometry of the 8-in schedule 40 test pipe. The 7- and 2-m pipe sections are connected by a 90° elbow with the bend radius being 1.5 times the outer diameter of the pipe. The defects introduced in the "forward" direction are highlighted and numbered in red. The distances given of the defects and weld in the forward direction are measured from the middle of the sensor.

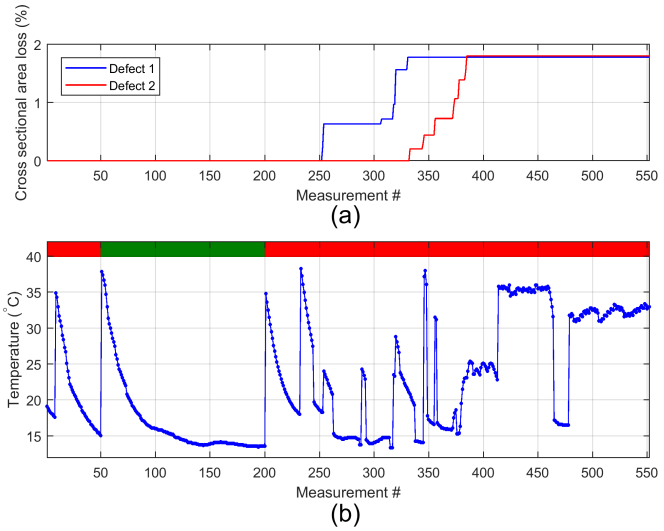

Fig. 3. (a) CSA losses due to the introduction of the defects. (b) Temperature of the pipe during the testing timeframe. Regions of low and high incoherent noise affecting the measurements are color-coded in green and red colors, respectively. The calibration signal set was chosen to be from measurements 51 to 200 (which are the ones indicated by the green bar).

outer diameter of the pipe), and the sensor was installed 4.5 m from the right-hand end in the figure. In addition to the elbow welds, there was a girth weld in the longer straight section of the pipe. The measurements used to perform the analysis reported in this article are the ones in the "forward" direction as indicated in Fig. 2. In that direction, two artificial defects were introduced during the testing timeframe by a manual grinding process to produce wall losses with circular/oval area profiles at each defect location. The defects were then gradually deepened in multiple stages by increasing the extent of the wall loss, giving the CSA losses as a function of measurement number (time) as shown in Fig. 3(a).

The pipe was subjected to heating and cooling cycles, with the temperature fluctuating between about 13 °C and 38 °C. Fig. 3(b) shows the temperature measured by a sensor installed on the pipe near the sensor ring. When analyzing the data, it was found that the instrumentation was set up to do insufficient averages to remove the incoherent noise and that this was higher in some sequences of measurements, which are indicated by the red bars in Fig. 3(b). This incoherent noise

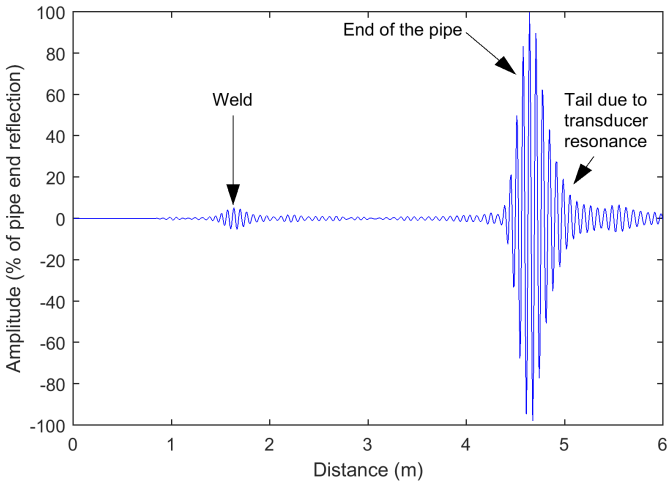

Fig. 4. Measurement #1 acquired at 19.1 °C and used as baseline for the PSC temperature compensation procedure [6].

was probably due to intermittent electromagnetic interference and was at a level that would normally be considered insignificant but became noticeable at the increased sensitivity levels obtained with the new compensation method presented in this article. In future, it will be straightforward to remove it with further shielding improvements or more averaging.

Fig. 4 shows the first measurement, which was acquired at 19.1 °C prior to the introduction of any defect. The time-domain ultrasonic signal is converted to distance in Fig. 4 using the known T(0, 1) velocity. Each signal was normalized to the reflection from the end of the pipe and was compensated for the temperature-dependent wave speed and transducer phase shift using the PSC procedure [6] described in the introduction, using the first measurement as the baseline.

The compensated (i.e., phase-shifted and time-stretched) signals are expected to exhibit well-aligned RF peaks, as seen, for example, in Fig. 5(a) where two signals recorded at temperatures of 36 °C and 20 °C are shown. The plot is zoomed in a portion of the pipe around the weld and shows excellent phase alignment throughout. However, the different coherent noise existing in different measurements still produces non-zero residuals even for measurements both taken on the undamaged structure, as seen in Fig. 5(b) where the residual between the two signals in Fig. 5(a) is plotted, hence making it more difficult to detect residuals due to the presence of a defect. The variation is somewhat worse using the BSS compensation procedure [25]. The differences between the two signals in Fig. 5(a) before the weld are likely to be primarily due to the interference between the circumferential A0- and S0-like modes, while after the weld there are also contributions from flexural modes reflected from the weld. The LSTC method specifically aims to compensate for these temperature-induced differences in coherent noise and, concurrently, for other phenomena as described in the next sections.

A. Results

The calibration signal set was chosen to be the cooling cycle from measurements 51 to 200, being the low incoherent noise region indicated by the green bar in Fig. 3(b). This choice

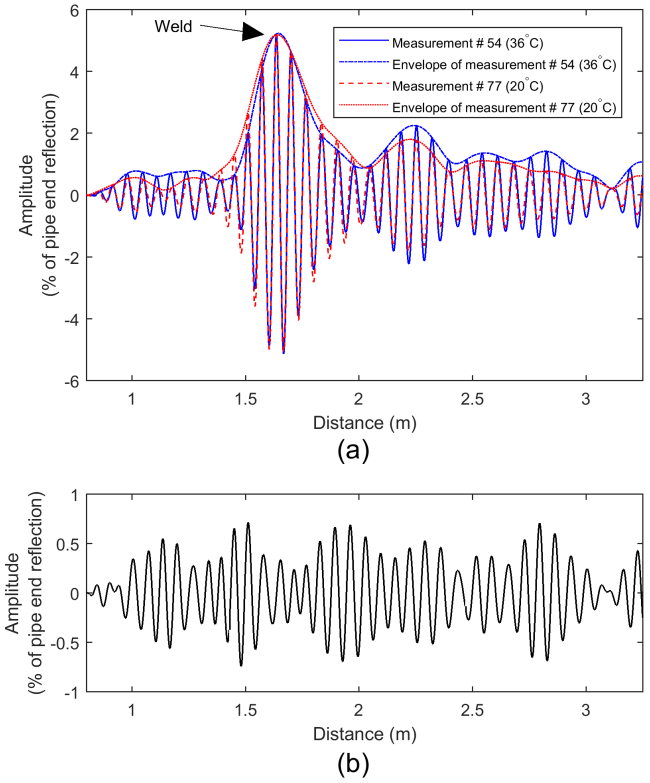

Fig. 5. (a) Signals acquired on undamaged pipe at 20 °C and 36 °C after PSC temperature compensation. (b) Residuals between the two measurements in (a). Note different vertical scales in (a) and (b).

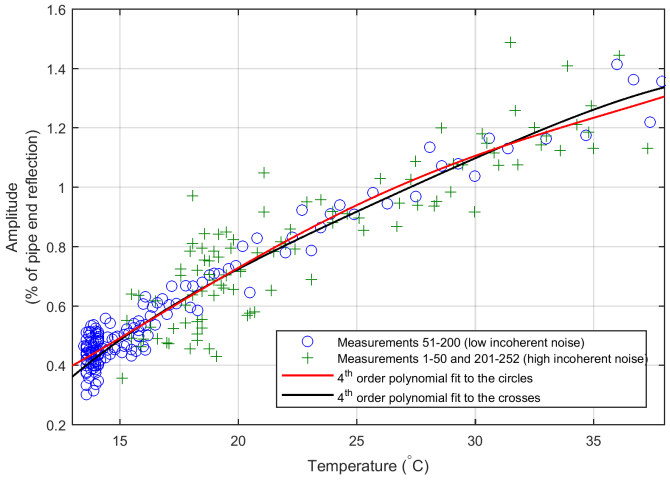

Fig. 6. Best-fit curves obtained for the axial position of 2.83 m when using as calibration signal set either measurements 51–200 (the low incoherent noise region) or the other defect-free measurements (the high incoherent noise region).

was primarily motivated by the fact that the temperature range spanned by that cooling cycle is the only one sufficiently wide to cover the temperature range of all the other measurements. At each axial position, a compensation curve of the signal amplitude against the temperature was computed by fitting the calibration data with fourth-order polynomials, as shown with blue circles and red curve for the axial location of 2.83 m in Fig. 6. Clearly, if a different cooling cycle were to be used, the resulting best-fit curves would be more prone to errors

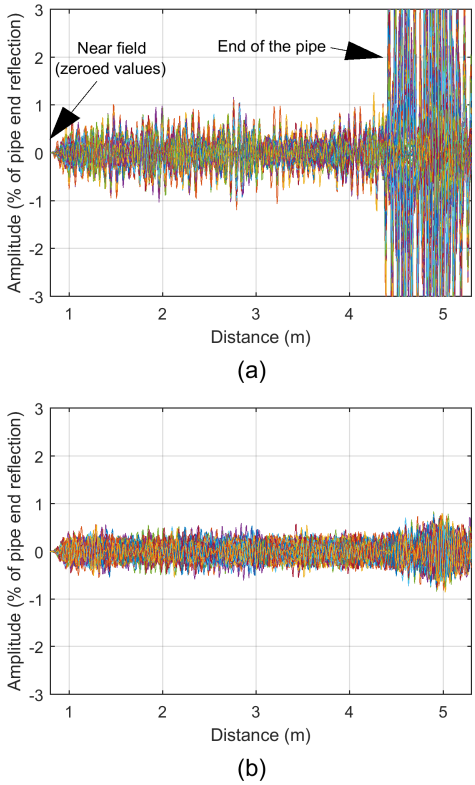

Fig. 7. (a) Residual signals obtained using the PSC and the baseline subtraction methods for measurements 2–252, i.e., before the first defect was introduced. (b) Compensation of measurements 1–252 using the new LSTC method performed by fitting fourth-order polynomials on the calibration signal set including measurements 51–200.

due to the higher variance of incoherent noise which affects the other measurements. However, using a sufficient number of measurements, the higher incoherent noise would smooth out; for example, Fig. 6 also shows the best-fit curve that is obtained when setting the calibration data to include the measurements in all the other cooling cycles before the introduction of any defect (i.e., measurements 1–50 and 201–252). As expected, the two curves almost overlap, and the green crosses representing the high incoherent noise measurements show higher variance around their fitting curve than the case of blue circles. The higher the incoherent noise in the acquired measurements, the higher the number of signals that would be necessary to include in the calibration set to protect against the random variations; at the levels of incoherent noise seen in measurements 51–200, only a few measurements spanning the temperature range of interest would be sufficient to correctly capture the variation in amplitude with temperature. In addition, in general, the wider the temperature range, the higher the value of n required to track the relationship in steps of 5 °C or less.

Fig. 7(a) shows the residuals obtained using the standard baseline subtraction method with PSC temperature compensation when processing the first 252 defect-free measurements (i.e., signal 1 subtracted from the signal obtained by PSC compensation applied to each of signals 2–252), the signals being overlaid on top of each other. Very high values of residuals are seen at the pipe end; because both the baseline and "current"

TABLE I
PEAK ABSOLUTE VALUES OF THE RESIDUAL SIGNALS OBTAINED USING THE PSC AND THE BASELINE SUBTRACTION METHODS [FIG. 7(A)] OR THE NEW LSTC METHOD [FIG. 7(B)]. FOR THE LATTER, THE RATIOS WITH RESPECT TO THE VALUES GIVEN BY THE PSC AND BASELINE SUBTRACTION METHODS ARE ALSO GIVEN. ONLY MEASUREMENTS 2–252 (BEFORE THE INTRODUCTION OF DEFECTS) ARE CONSIDERED

	Before pipe end reflection (% pipe end reflection)	At pipe end reflection (% pipe end reflection)
PSC and baseline subtraction	1.266	11.931
LSTC	0.61 (51.8% reduction)	0.856 (92.8% reduction)

signals contain large components of the pipe end reflection, the baseline subtraction involves subtracting two large quantities and, therefore, is very sensitive to environmentally induced signal changes. These include frequency response changes of the transducers, such as ringing effects (e.g., the signal tail at 19.1 °C shown in Fig. 4), and the "frequency noise" as discussed above. For comparison, Fig. 7(b) shows the residual signals output by the LSTC method when processing the same 252 defect-free measurements, and the maximum absolute values of the residuals obtained for the two sets of results with and without including the pipe end reflections are given in Table I. The residuals output by the LSTC method are lower than those obtained by the standard baseline subtraction, with more than an order of magnitude improvement at the pipe end, where, as reported in Table I, the peak residual is about 7.2% of that given by the standard technique; this shows that the LSTC procedure also compensates for both frequency response changes of the transducers and "frequency noise." Clearly, the reduction in residuals enabled by the LSTC over the standard baseline subtraction method also depends on the range of temperatures over which the measurements are acquired, with the benefits expected to increase as the temperature range increases.

The reduction in residuals produced by the new LSTC method to below 0.6% of the pipe end reflection at locations away from the pipe end means that defects removing around 1% of the CSA would be detectable in a single test, with further improvements likely using multiple readings [9], [16]. Even close to the pipe end, it would be possible to detect a defect removing about 1.5% CSA in a single test.

B. Trends of Data Acquired at Each Pipe Location

Fig. 8 shows the progression of residuals obtained over the whole set of 552 signals at two different axial positions in defect-free areas of the pipe [i.e., not affected by reflections from either of the two defects whose growth is shown in Fig. 3(a)]. Fig. 8(a)–(c) refers to the point at 1.45 m, which is before the weld and so the coherent noise is primarily due to the circumferential modes, while Fig. 8(d)–(f) shows the case of the point at 4.38 m, which is close to the end of the pipe. Fig. 8(b) and (e) shows the temperature readings [the same plot as in Fig. 3(b)] alongside the residuals obtained using the baseline subtraction method with PSC temperature compensation. There is a clearly strong correlation between the trends of the residuals and the temperature variation. Fig. 8(a) and (d) shows the scatter plots of the calibration data for the LSTC method at the two locations, which were taken from measurements 51 to 200 as discussed in the previous section, together with the fourth-order polynomial curves which best-fit the data of each plot. The LSTC procedure produced the residuals as shown in Fig. 8(c) and (f), which show no sign of temperature dependence and which are randomly distributed about zero. The degree to which the residuals output by the LSTC procedure fit a normal distribution was checked by applying the Lilliefors test [31]. At the point at 1.45 m [Fig. 8(c)], the data in the low incoherent noise region (measurements 51–200) yielded a p-value of 0.65 and those in the high incoherent noise regions (measurements 1–50 and 201–552) gave a p-value of 0.63, thus both comfortably passing the normality test at a 5% significance level which requires the p-value to be greater than 0.05 [32]. Similarly, at the point at 4.38 m [Fig. 8(f)], p-values of 0.96 and 0.82 were obtained in the same two measurement regions. The lower fluctuations would make it much easier to detect small defects reliably and the normal distribution implies that averaging over multiple readings could be used to further reduce the uncertainty. The residual fluctuations are mostly due to the random effects of the incoherent noise, as shown by the lower residuals in Fig. 8(c) and (f) over measurements 51–200 where the incoherent noise was lower as indicated in Fig. 3(b).

Fig. 8(f) also shows that if a defect occurs somewhere along the pipe, the modified geometry at the defect location changes the transmitted signal at all points past this location, so the LSTC procedure no longer gives very low residuals, making defect calling past the first defect less reliable; this is particularly true when the first defect is large, so the perturbation in the transmitted signal is also large. For the point at 4.38 m of Fig. 8(f), after measurement 385, when both defects 1 and 2 reached their maximum sizes [Fig. 3(a)], the trends are clearly seen to deviate from the zero-mean. A rather more severe case of a fitting curve being invalidated by the changed pipe geometry is shown in Fig. 9(f), which is discussed below.

Fig. 9 shows the cases of two pipe locations featuring reflections from the two defects. Fig. 9(a)–(c) refers to the location of defect 2 at 2.76 m, while Fig. 9(d)–(f) shows the location of defect 1 at 3.59 m. The plots are analogous to those of Fig. 8, and Fig. 9(b), (c), (e), and (f) also shows the evolution of the cross-sectional losses produced by the defects, these curves being the same as those in Fig. 3(a). In Fig. 9(c), the LSTC method outputs a flat trend before measurement 333, that is, when defect 2 was introduced. In contrast, over the same measurement range, the baseline subtraction method of Fig. 9(b) gives the variations in the order of 1% of the pipe end reflection. The presence of these variations when the pipe is undamaged hinders the positive detection of the reflection given by the defect, especially in its early stages of growth (i.e., when the CSA loss is below 1%). In contrast,

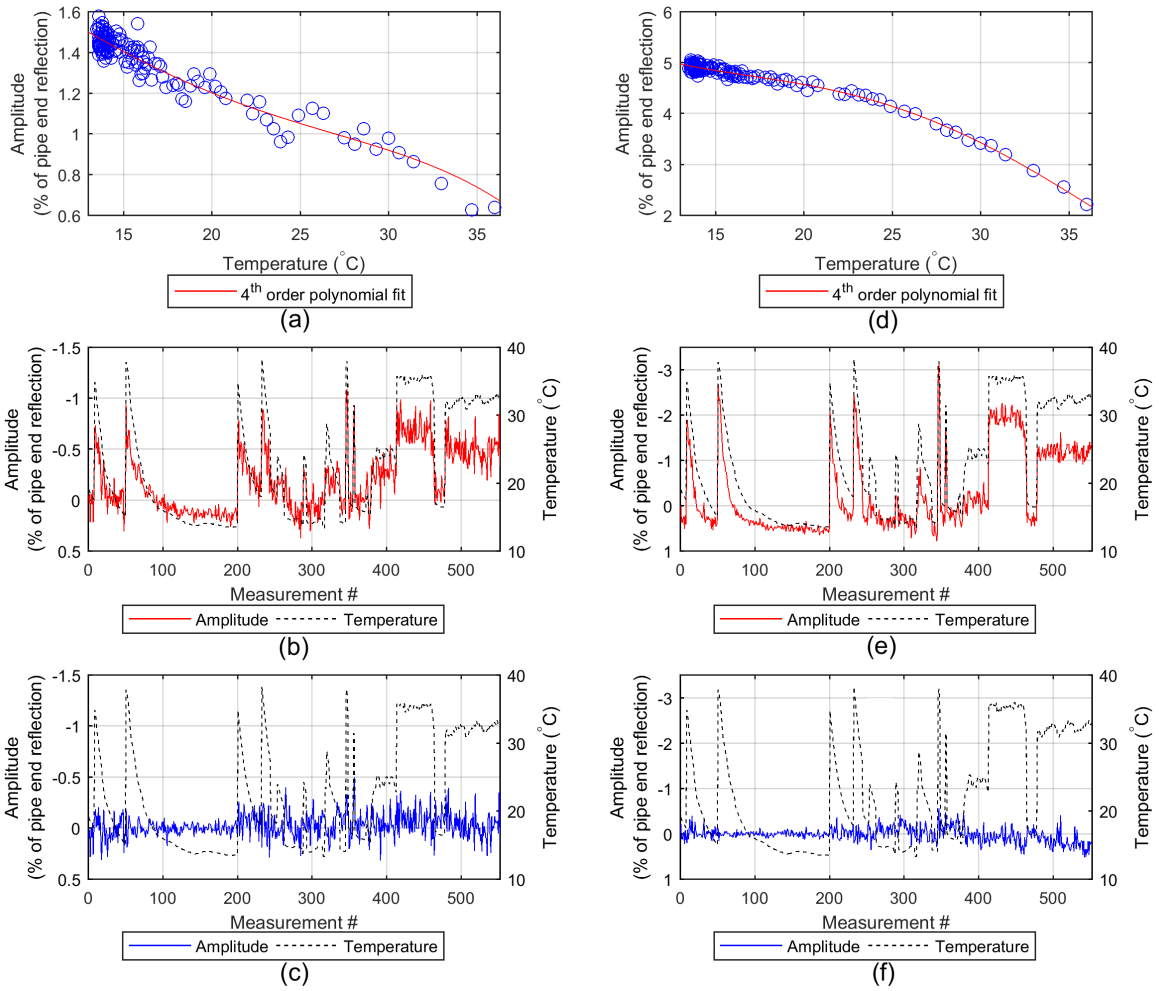

Fig. 8. Results at locations with no defect growth. (a)–(c) Point at 1.45 m (before the weld). (d)–(f) Point at 4.38 m (first arrival of the reflection from the pipe end). (a) and (d) Calibration data for LSTC method and best-fit curves. (b) and (e) Temperature readings and residuals obtained using the baseline subtraction method with PSC temperature compensation. (c) and (f) Residuals output by the LSTC method.

the LSTC results correctly track the known defect growth at all stages, hence enabling reliable, early detection. Note that for the T(0, 1) mode, the reflection ratio from a defect (calculated as the amplitude of the reflected wave divided by the amplitude of the incident wave) is roughly equal to the CSA loss, with the ratio between the axial extent of the defect and wavelength also affecting the reflection ratio [33]; this causes the slight discrepancy seen between the blue and green curves in Fig. 9(c), especially after measurement ∼360.

Fig. 9(d) shows that at the axial location of defect 1, the effect of temperature variations on the coherent noise when the pipe was in its initial state was small, the range of the values spanned by the fitting curve being only around 0.3% of the pipe end reflection for the temperatures of interest. For this reason, the plot given by the baseline subtraction method in Fig. 9(e) already shows low variations due to temperature, and no significant improvements are obtained by the application of the LSTC method, as seen in Fig. 9(f). Therefore, both plots correctly track the growth of defect 1 after its introduction at measurement 253 up to measurement 333, when defect 2 was introduced. After that measurement, the modified pipe geometry due to the introduction of defect 2 (which is located between the sensor and the location of defect 1 to which the plot refers) made both the standard baseline subtraction and LSTC methods based on the pre-damage measurements less accurate, as discussed above.

The effects of changing temperature on the coherent noise at the different axial positions vary from one location to another. Fig. 10(a) shows the range of values spanned by the fitting curve computed at each pipe location for temperatures ranging from 13 °C to 37 °C. The high-frequency oscillations seen in the figure are due to the varying phase of the RF signal. The higher the range of the variation with temperature, the greater the benefit derived from the application of the LSTC method. Fig. 10(b) shows the residual signals output by the LSTC method when processing all the 552 measurements (analogous to Fig. 7(b), where only the 252 defect-free measurements were plotted). The waves reflected by the two defects at their full growth are clearly seen protruding well above the noise floor. Because the RF peak of the wave reflected by defect 2 occurs at 2.76 m, where the temperature-induced coherent noise variations are high [about 0.9% of the pipe end

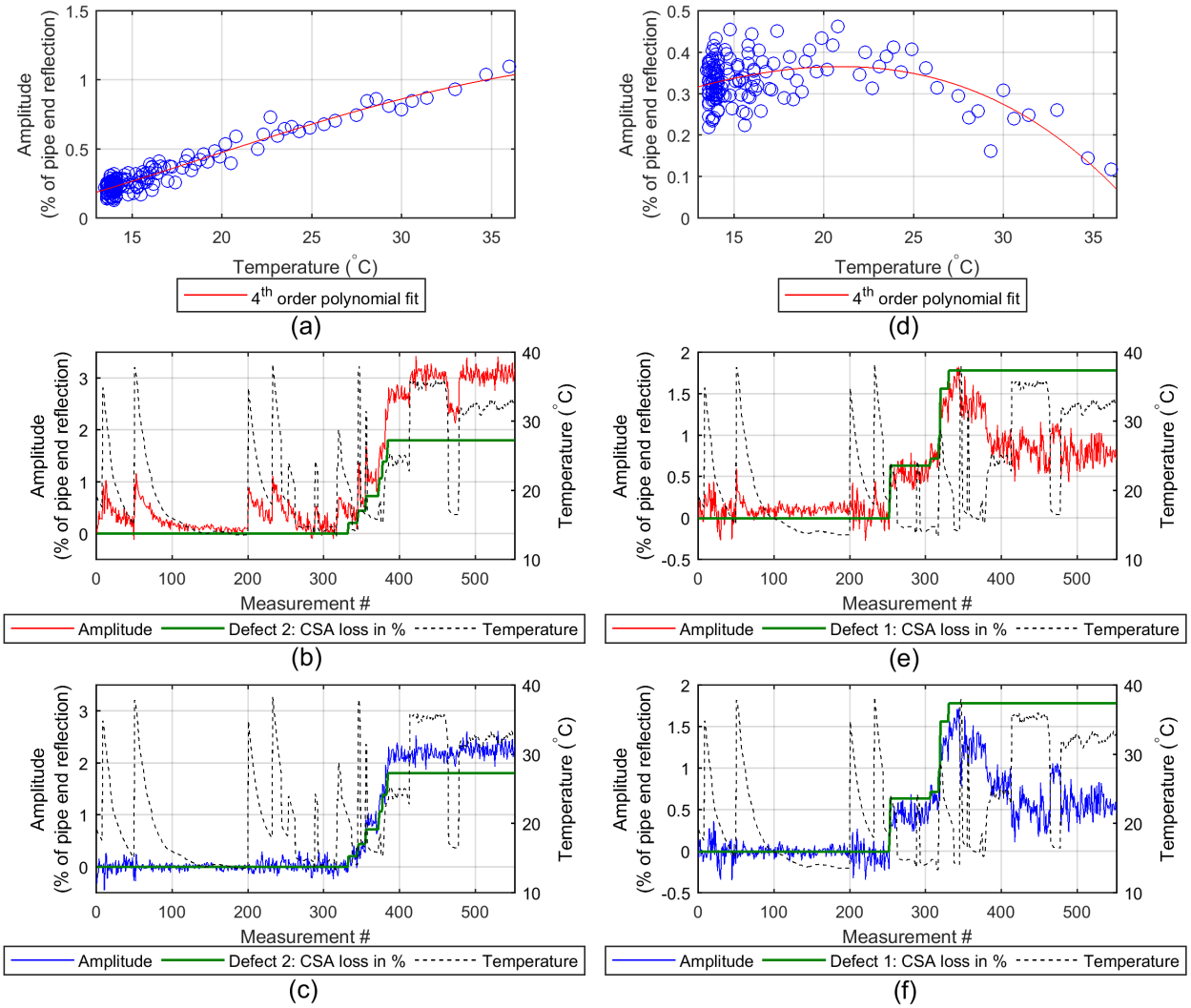

Fig. 9. (a)–(c) Point at 2.76 m (defect 2 maximum reflection). (d)–(f) Point at 3.59 m (defect 1 maximum reflection). (a) and (d) Calibration data for the LSTC method and best-fit curves. Note the different amplitude scales in the two plots. (b) and (e) Temperature readings and residuals obtained using the baseline subtraction method with PSC temperature compensation; the CSA losses in % of the pipe end reflection due to the introduction of the two defects are also shown. (c) and (f) Residuals output by the LSTC method; the CSA losses are also shown.

reflection, as seen in Fig. 10(a)], the benefit of using LSTC for the detection of this defect is higher than that for the case of defect 1, whose reflected wave has a peak occurring at a location where the effects of temperature on the coherent noise are marginal. Fig. 10(b) also shows significant peaks at the end of the pipe; these are largely caused by the reduction in the amplitude of the input torsional wave signal reaching the end of the pipe due to reflections from the defects introduced between the sensor and the pipe end.

C. Compensation of Attenuation

The distance–amplitude correction (DAC) curves are typically used in bulk wave and guided wave inspection to account for attenuation of the transmitted signal along the testpiece so that a given size of reflector will produce the same signal amplitude, irrespective of its distance from the transducer [2], [34]; if the attenuation is due to material damping, the DAC curve will be an exponential. However, in guided wave inspection, transmission reduction due to reflections from features such as welds produces step changes in the DAC curves, in addition to the exponential changes between them. This can be accommodated by assuming that all welds produce a similar transmission loss, or can more accurately be accounted for using knowledge of the weld geometry and modeling it to obtain a predicted reflection. For a given pipeline, the extent of attenuation and the shape of the DAC curve are influenced by factors such as operating temperature, pipe contents, coating, and level of generalized corrosion, so that a different DAC curve would have to be computed for each reading. This can be a complicated task, especially when there is no clear reflector at the end of the interrogated section.

In many cases, the DAC curve will be temperature dependent due to, for example, a viscous coating on the pipe or a viscous liquid filling the pipe. The LSTC method automatically compensates for any such temperature-dependent effect. Because the uncoated, empty pipe of Fig. 2 showed minimal attenuation, we illustrate this through a synthetic data set showing temperature-dependent attenuation. Each of the

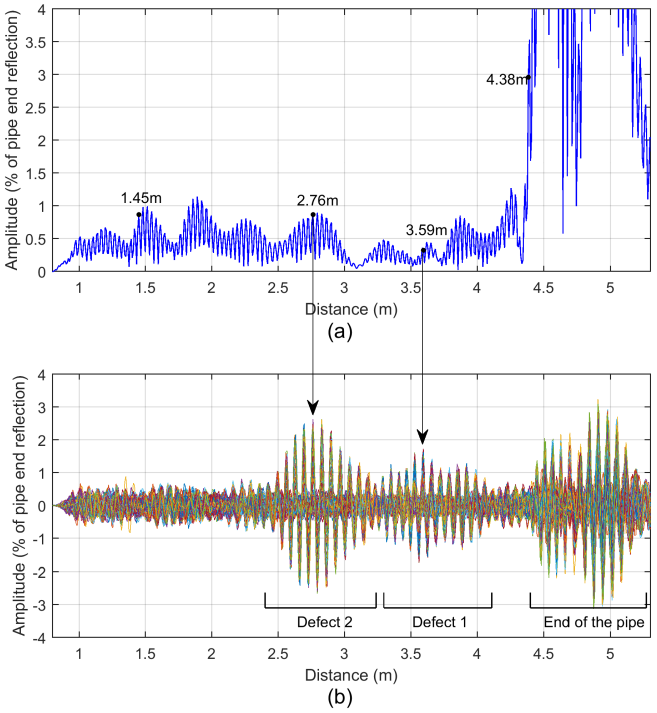

Fig. 10. (a) Range of values spanned by the fitting curve computed at each pipe location for temperatures ranging from 13 °C to 37 °C. The axial positions investigated in Figs. 8 and 9 are highlighted. (b) Results from the LSTC method from all the measurements. The positions corresponding to the reflections from the two defects and the pipe end are indicated.

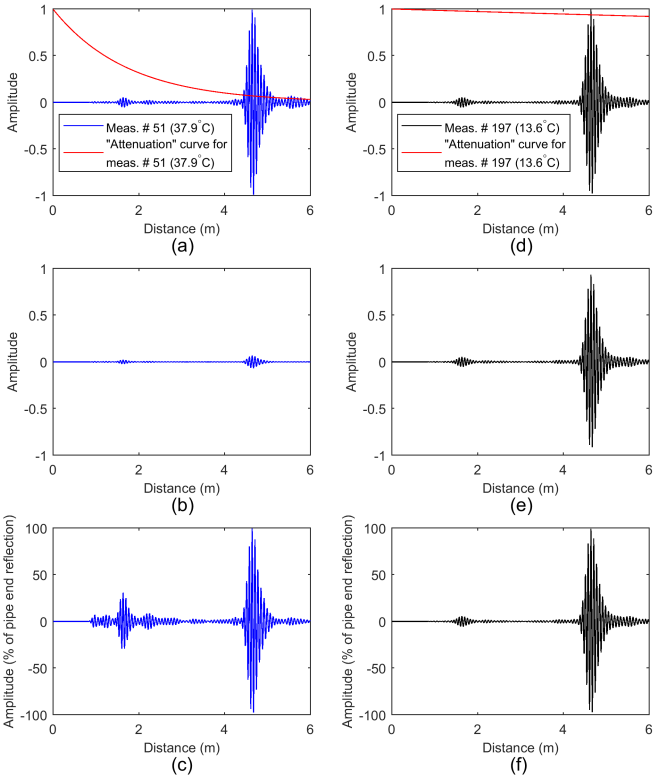

Fig. 11. Synthetic signals obtained by applying temperature-dependent levels of attenuation to measurements 51 and 197, acquired at temperatures of 37.9 °C and 13.6 °C, respectively. (a) and (d) Actual measurements with the hypothetical attenuation curve corresponding to the pipe temperature. (b) and (e) Synthetic signals including the simulated attenuation. (c) and (f) Synthetic signals after normalizing to the pipe end reflection.

552 measurements in the forward direction of Fig. 2 was multiplied by an exponential function of the form

$$f(d, T) = e^{-\alpha(T)\cdot d} \tag{1}$$

where T is the temperature, d is the distance from the sensor, and $\alpha(T)$ is an arbitrarily chosen damping factor, such that it increases linearly with increasing temperature [examples of "high" and "low" levels of attenuations are shown in Fig. 11(a) and (d), respectively]. Fig. 11 illustrates the process applied to measurements 51 and 197, acquired at temperatures of 37.9 °C and 13.6 °C, respectively. The measurements shown in Fig. 11(a) and (d) were multiplied by the appropriate attenuation curve expressed by (1) giving the signals shown in Fig. 11(b) and (e); these were then normalized to the pipe end reflection as seen in Fig. 11(c) and (f). Substantial differences are seen in the signal amplitude distribution along the pipe due to the simulated attenuation (e.g., the weld reflection at 1.5 m changes from 6% to 31% of the end reflection).

Fig. 12 shows the points at 1.45 and 4.38 m, that is, the same pipe locations illustrated in Fig. 8. The calibration data, and hence the best-fit curves of Fig. 12(a) and (d), show higher rates of decay with temperature than those of Fig. 8(a) and (d), due to the additional effect of the synthetically imposed attenuation. As expected, the baseline subtraction method with PSC temperature compensation produced residuals strongly correlated with the temperature, as shown in Fig. 12(b) and (e), while the LSTC procedure yielded residuals de-coupled from temperature variations and randomly distributed about zero, as seen in Fig. 12(c) and (f).

D. LSTC Method Applied to Independent Component Analysis Processed Data

There has been recent interest in applying the component analysis methods to SHM time series data using SVD [14] or ICA [15]. This enables dimensionality reduction and may also help separate defect growth from other effects. It is, therefore, of interest to investigate whether the new LSTC compensation method can be used in conjunction with the component analysis techniques. The component analysis algorithms decompose the data matrix X that contains the measurements over time into the form

$$\boldsymbol{X} = \boldsymbol{W}\boldsymbol{A}^T \tag{2}$$

where $\boldsymbol{W}$ and $\boldsymbol{A}$ are the matrices containing the weights and the components of $\boldsymbol{X}$, respectively. $\boldsymbol{X}$ is an $N \times D$ data matrix, where N is the number of signals measured over the monitoring period (e.g., 552 measurements for the example considered in this article) and D is the number of sample points in each signal. The weight matrix, $\boldsymbol{W}$, has dimensions $N \times R$ and the component matrix, $\boldsymbol{A}$, has dimensions $D \times R$ with $R \ll N, D$, hence giving the reduced dimensionality. Each column of $\boldsymbol{W}$ ($\boldsymbol{w}^{N\times 1}$) represents the trend over time

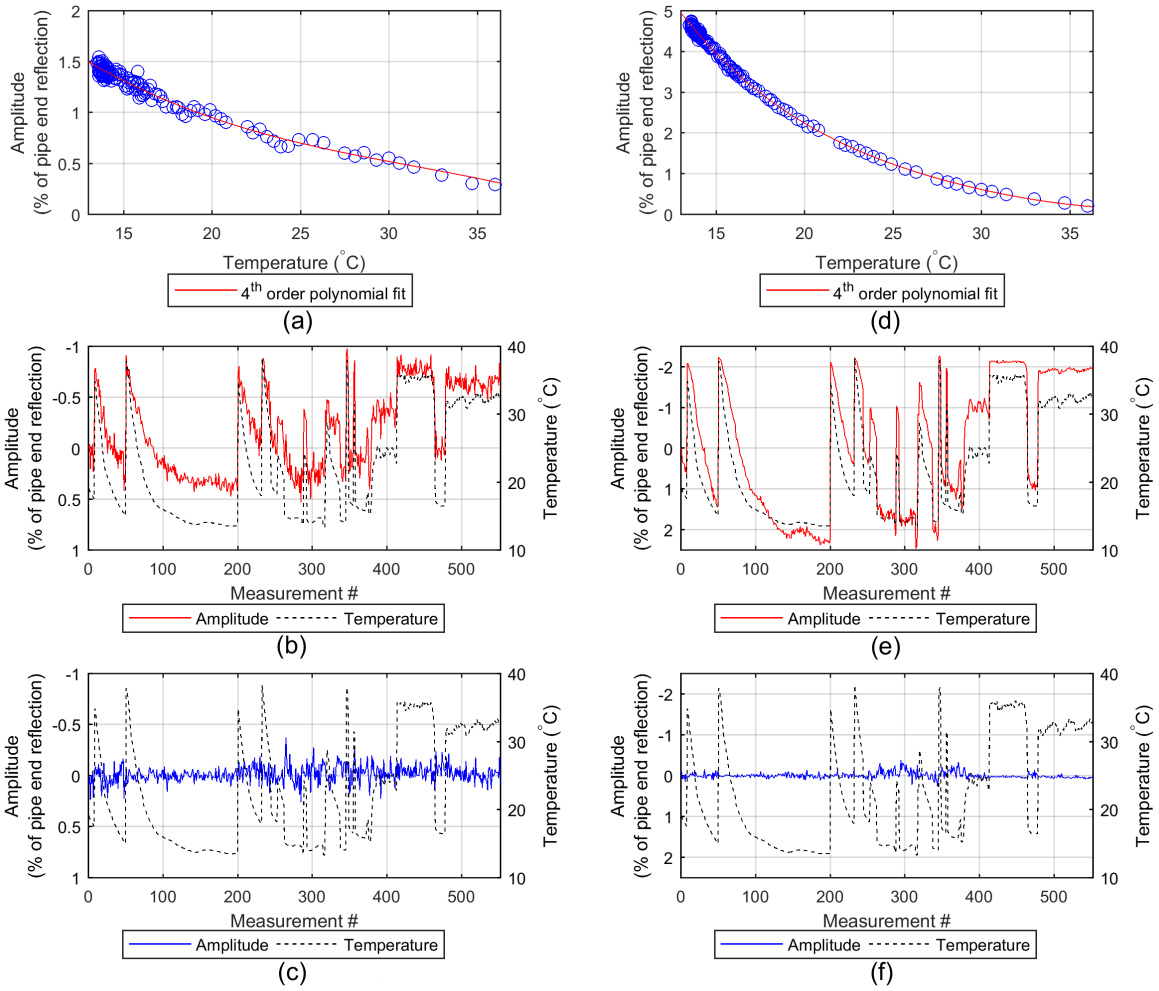

Fig. 12. Results from the data set corrupted with simulated attenuation. (a)–(c) Point at 1.45 m (before the weld). (d)–(f) Point at 4.38 m (first arrival of the reflection from the pipe end). (a) and (d) Calibration data for the LSTC method and best-fit curves. (b) and (e) Temperature readings and residuals obtained using the baseline subtraction method with PSC temperature compensation. (c) and (f) Residuals output by the LSTC method.

corresponding to one signal component, this being a column of $\boldsymbol{A}$ ($\boldsymbol{a}^{R\times 1}$).

The LSTC method can be directly applied to the weights produced by this type of algorithm. For example, Fig. 13 shows the case of a component obtained by applying ICA to the 552 PSC-compensated signals that were acquired as in Fig. 3(b). Fig. 13(a) shows the envelope of this component, whose energy is centered on the point analyzed in Fig. 9(a)–(c), and hence affected by the reflections from defect 2. Fig. 13(c) shows the associated weight function, which starts at a set value of zero and then varies over time with a strong correlation to temperature, as well as to the defect after its introduction. As shown previously, readings 51–200 of the weight function were used to obtain the calibration function for the LSTC method shown in Fig. 13(b); the compensated weight function in Fig. 13(d) only shows low-amplitude variations before the introduction of the defect and closely follows the trend of the CSA loss after the defect was introduced; as in Fig. 9(c), the compensated weight function exceeds the cross-sectional loss after around measurement 360. Both the weight function shown in Fig. 13(c) and the results from the LSTC procedure in Fig. 13(d) are in good agreement with the progression of residuals shown in Fig. 9(b) and (c), respectively.

IV. Conclusion

The use of PIMSs for SHM of pipes (or other structures) has the potential to enable detection of damage at earlier stages than when using the one-off inspection systems. In a typical PIMS setting, the residuals are obtained using the baseline subtraction method, where an earlier measurement is subtracted from the "current" signal. The goal is to minimize the residuals in the absence of defects so that when a defect occurs, it can easily be identified by detecting high residual values due to partial signal reflections. Unfortunately, this procedure is hindered by the effects of changing EOCs, for example, temperature, which produce changes in the coherent noise affecting the signals.

Many temperature compensation methods have been developed, which typically involve stretching the whole signal to compensate for the variation in wave speed induced by a change in temperature. However, these "global" methods

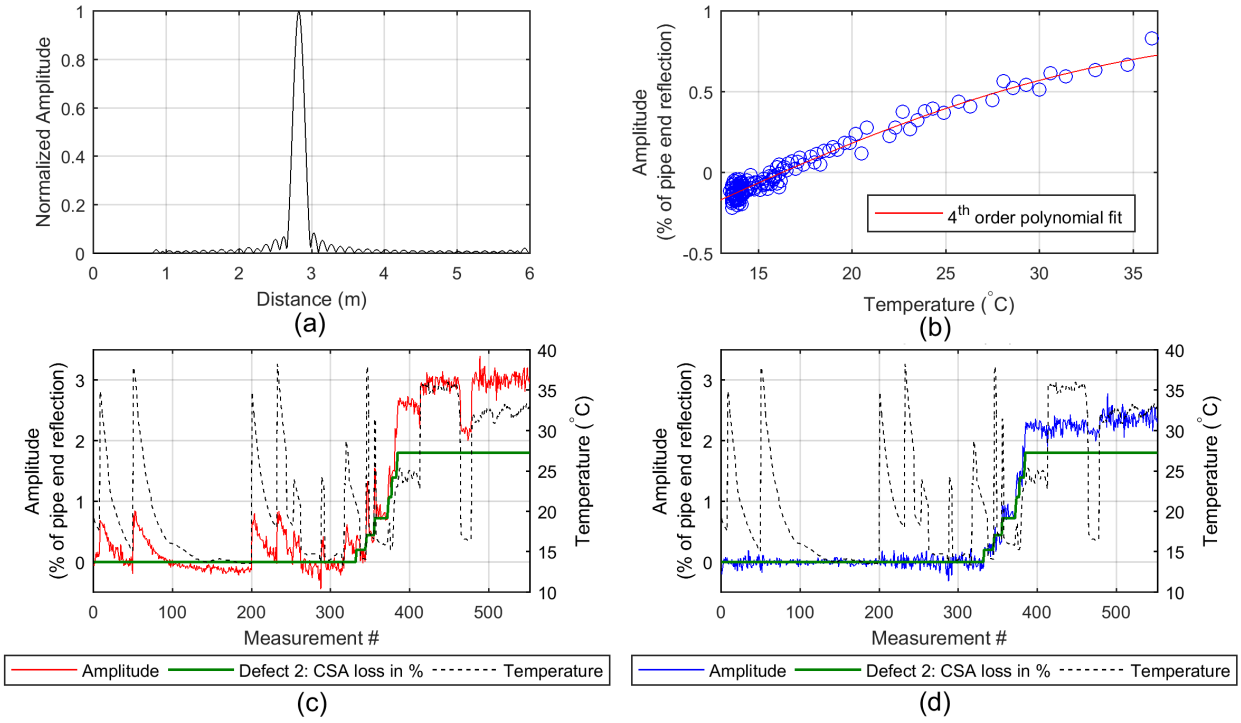

Fig. 13. ICA component centered at 2.76 m (defect 2). (a) Envelope of the component. (b) Calibration data for the LSTC method and best-fit curve. (c) Weight function. (d) Compensated weight function output by the LSTC method.

cannot target spatially dependent signal changes such as those due to the changes in the mix of modes excited by the transduction system or the changes in the interference pattern of unwanted modes propagating in the structure. Removal of these effects requires a compensation method that is position dependent. Therefore, this article introduced an LSTC procedure that after the application of a "global" method such as BSS or PSC is used to adjust the signal at each position so that in the absence of a defect, the residual is reduced to close to zero. The assumption is that the changes in coherent noise are a function of temperature that does not vary with time; hence, the inspection system is required to guarantee good transducer stability over the testing timeframe. Under these conditions, at each position, a calibration function that models the variation in coherent noise with temperature is computed from a set of baseline signals and is used to correct the measurements.

The new LSTC method was applied to a data set of guided wave signals collected by a PIMS installed on a pipe and using the T(0, 1) wave mode. The results show that the LSTC method gives lower residuals than the conventional baseline subtraction approach, yielding at least 50% reduction away from features and more than 90% reduction at features such as the pipe end. Furthermore, the residuals are de-coupled from temperature variations and, in absence of defects, normally distributed around zero, thus facilitating the identification of trends over time and enabling the use of statistical change-detection methods such as those used in quality control [32]. It has also been shown that the method can be successfully applied directly either to the guided wave signals or to the weights of the components extracted by the ICA or other component analysis methods. Furthermore, the method is computationally inexpensive. For example, when it was directly applied to the 552 guided wave measurements of the data set used in this article, where each signal consisted of 740 samples, the computation required ~2 s on a PC of average performance (i.e., ~3.6 ms per signal).

The LSTC method automatically compensates for any signal change that is a systematic function of temperature; other than the already-cited effects of modified balance of unwanted modes, this includes signal changes due to frequency response changes, the "frequency noise" effect, mirror artifacts produced by reflections of the signal traveling in an unwanted direction as a result of imperfect direction control due to varying wavelength, and the variations in attenuation causing changes that increase with distance from the source. It is believed that the method is equally applicable to conventional ultrasonic testing applications using bulk waves or to other types of guided wave inspection systems. Furthermore, it is suggested that an analogous procedure can be derived to compensate for ultrasonic signal changes due to loads on the testpiece, in which case the calibration curves of the signal amplitude against the load can be computed and used to correct the measurements; by extension, calibration surfaces can be used to compensate for the concurrent effects of temperature and load. The LSTC method is the subject of a patent application [35].

Acknowledgment

The authors would like to thank Guided Ultrasonics Ltd., Brentford, U.K., and HOIS (a joint-industry project managed by ESR Technology) for providing the experimental data.

REFERENCES

[1] P. Cawley, F. Cegla, and M. Stone, "Corrosion monitoring strategies—Choice between area and point measurements," *J. Nondestruct. Eval.*, vol. 32, no. 2, pp. 156–163, Jun. 2013.

[2] P. Cawley, M. J. Lowe, D. N. Alleyne, B. Pavlakovic, and P. Wilcox, "Practical long range guided wave inspection-applications to pipes and rail," *Mater. Eval.*, vol. 61, no. 1, pp. 66–74, 2003.

[3] D. N. Alleyne and P. Cawley, "The excitation of Lamb waves in pipes using dry-coupled piezoelectric transducers," *J. Nondestruct. Eval.*, vol. 15, no. 1, pp. 11–20, Mar. 1996.

[4] D. Gridin, R. V. Craster, J. Fong, M. J. S. Lowe, and M. Beard, "The high-frequency asymptotic analysis of guided waves in a circular elastic annulus," *Wave Motion*, vol. 38, no. 1, pp. 67–90, Jun. 2003.

[5] D. N. Alleyne, M. J. S. Lowe, and P. Cawley, "The reflection of guided waves from circumferential notches in pipes," *J. Appl. Mech.*, vol. 65, no. 3, pp. 635–641, Sep. 1998.

[6] S. Mariani, S. Heinlein, and P. Cawley, "Compensation for temperature-dependent phase and velocity of guided wave signals in baseline subtraction for structural health monitoring," *Struct. Health Monit.* to be published. doi: 10.1177/1475921719835155.

[7] V. M. N. Ledesma, E. P. Baruch, A. Demma, and M. J. S. Lowe, "Guided wave testing of an immersed gas pipeline," *Mater. Eval.*, vol. 67, no. 2, pp. 102–115, 2009.

[8] P. Cawley, F. Cegla, and A. Galvagni, "Guided waves for NDT and permanently-installed monitoring," *Insight Non Destructive Test. Condition Monit.*, vol. 54, no. 11, pp. 594–601, 2012.

[9] S. Heinlein, P. Cawley, T. Vogt, and S. Burch, "Blind trial validation of a guided wave structural health monitoring system for pipework," *Mater. Eval.*, vol. 76, no. 8, pp. 1118–1126, 2018.

[10] A. Dhutti, J. Kanfoud, T.-H. Gan, B. Hernandez, and P. Mudge, "iPerm: A guided wave pipeline monitoring tool for the oil & gas industry," in *Proc. 9th Eur. Workshop Struct. Health Monit. (EWSHM)*, 2018. [Online]. Available: https://www.ndt.net/article/ewshm2018/papers/0347-Gan.pdf

[11] B. Herdovics and F. Cegla, "Structural health monitoring using torsional guided wave electromagnetic acoustic transducers," *Struct. Health Monitor.*, vol. 17, no. 1, pp. 24–38, 2018.

[12] S. Vinogradov, T. Eason, and M. Lozev, "Evaluation of magnetostrictive transducers for guided wave monitoring of pressurized pipe at 200 °C," *J. Press. Vessel Technol.*, vol. 140, no. 2, p. 21603, Feb. 2018.

[13] A. J. Croxford, P. D. Wilcox, B. W. Drinkwater, and G. Konstantinidis, "Strategies for guided-wave structural health monitoring," *Proc. Roy. Soc. A, Math. Phys. Eng. Sci.*, vol. 463, no. 2087, pp. 2961–2981, Nov. 2007.

[14] C. Liu, J. B. Harley, M. Bergés, D. W. Greve, and I. J. Oppenheim, "Robust ultrasonic damage detection under complex environmental conditions using singular value decomposition," *Ultrasonics*, vol. 58, pp. 75–86, Apr. 2015.

[15] J. Dobson and P. Cawley, "Independent component analysis for improved defect detection in guided wave monitoring," *Proc. IEEE*, vol. 104, no. 8, pp. 1620–1631, Aug. 2016.

[16] C. Liu, J. Dobson, and P. Cawley, "Efficient generation of receiver operating characteristics for the evaluation of damage detection in practical structural health monitoring applications," *Proc. Roy. Soc. A, Math. Phys. Eng. Sci.*, vol. 473, Mar. 2017, Art. no. 20160736.

[17] S. Heinlein, P. Cawley, and T. Vogt, "Validation of a procedure for the evaluation of the performance of an installed structural health monitoring system," *Struct. Health Monit.*, vol. 18, nos. 5–6, pp. 1557–1568, 2019.

[18] R. L. Weaver and O. I. Lobkis, "Temperature dependence of diffuse field phase," *Ultrasonics*, vol. 38, nos. 1–8, pp. 491–494, Mar. 2000.

[19] H. Sohn, "Effects of environmental and operational variability on structural health monitoring," *Philos. Trans. A, Math. Phys. Eng. Sci.*, vol. 365, no. 1851, pp. 539–560, Feb. 2007.

[20] T. Clarke, F. Simonetti, and P. Cawley, "Guided wave health monitoring of complex structures by sparse array systems: Influence of temperature changes on performance," *J. Sound Vib.*, vol. 329, no. 12, pp. 2306–2322, Jun. 2010.

[21] Y. Lu and J. E. Michaels, "A methodology for structural health monitoring with diffuse ultrasonic waves in the presence of temperature variations," *Ultrasonics*, vol. 43, no. 9, pp. 717–731, Oct. 2005.

[22] G. Konstantinidis, P. D. Wilcox, and B. W. Drinkwater, "An investigation into the temperature stability of a guided wave structural health monitoring system using permanently attached sensors," *IEEE Sensors J.*, vol. 7, no. 5, pp. 905–912, May 2007.

[23] A. J. Croxford, P. D. Wilcox, G. Konstantinidis, and B. W. Drinkwater, "Strategies for overcoming the effect of temperature on guided wave structural health monitoring," *Proc. SPIE*, vol. 6532, May 2007, Art. no. 65321T.

[24] A. J. Croxford, J. Moll, P. D. Wilcox, and J. E. Michaels, "Efficient temperature compensation strategies for guided wave structural health monitoring," *Ultrasonics*, vol. 50, nos. 4–5, pp. 517–528, 2010.

[25] J. B. Harley and J. M. F. Moura, "Scale transform signal processing for optimal ultrasonic temperature compensation," *IEEE Trans. Ultrason., Ferroelectr., Freq. Control*, vol. 59, no. 10, pp. 2226–2236, Oct. 2012.

[26] S. Ha, K. Lonkar, A. Mittal, and F.-K. Chang, "Adhesive layer effects on PZT-induced Lamb waves at elevated temperatures," *Struct. Health Monit.*, vol. 9, no. 3, pp. 247–256, May 2010.

[27] S. Roy, K. Lonkar, V. Janapati, and F.-K. Chang, "A novel physics-based temperature compensation model for structural health monitoring using ultrasonic guided waves," *Struct. Health Monit.*, vol. 13, no. 3, pp. 321–342, May 2014.

[28] B. Herdovics and F. Cegla, "Compensation of phase response changes in ultrasonic transducers caused by temperature variations," *Struct. Health Monit.*, vol. 18, no. 2, pp. 508–523, 2018.

[29] R. Jarvis, "Current deflection NDE for pipe inspection and monitoring," Ph.D. dissertation, Imperial College London, London, U.K., 2017.

[30] *Guided Ultrasonics Ltd*. Accessed: Aug. 22, 2018. [Online]. Available: https://www.guided-ultrasonics.com/

[31] H. W. Lilliefors, "On the Kolmogorov–Smirnov test for normality with mean and variance unknown," *J. Amer. Stat. Assoc.*, vol. 62, no. 318, pp. 399–402, Jun. 1967.

[32] D. C. Montgomery, *Introduction to Statistical Quality Control*, 6th ed. Hoboken, NJ, USA: Wiley, 2009, pp. 116–117.

[33] A. Demma, P. Cawley, M. Lowe, and A. G. Roosenbrand, "The reflection of the fundamental torsional mode from cracks and notches in pipes," *J. Acoust. Soc. Amer.*, vol. 114, no. 2, pp. 611–625, Aug. 2003.

[34] J. Krautkrämer and H. Krautkrämer, *Ultrasonic Testing of Materials*, 4th ed. Berlin, Germany: Springer, 1990.

[35] S. Mariani, "Signal processing," U.K. Patent 1815256.1, Sep. 19, 2018.

Stefano Mariani received the Laurea Specialistica degree in structural engineering from the University of Perugia, Perugia, Italy, in 2010, and the Ph.D. degree in structural engineering from the University of California at San Diego, San Diego, CA, USA, in 2015.

He is currently a Research Associate with the Non-Destructive Testing Group, Imperial College London, London, U.K. His research interest includes guided wave testing and using statistical methods for structural health monitoring.

Sebastian Heinlein was born in Frankfurt, Germany, in 1991. He received the B.Sc. degree in physics from the University of Warwick, Coventry, U.K., in 2014, and the Eng.D. degree in nondestructive evaluation from Imperial College London, London, U.K., in 2019.

In 2018, he joined Guided Ultrasonics Ltd., Brentford, U.K., as a Data Analytics Development Engineer continuing his work on guided wave testing and structural health monitoring.

Peter Cawley was born in Sheffield, U.K., in 1953. He received the B.Sc. and Ph.D. degrees in mechanical engineering from the University of Bristol, Bristol, U.K., in 1975 and 1979, respectively.

From 1979 to 1981, he worked in industry and later joined the Mechanical Engineering Department, Imperial College, London, U.K., as a Lecturer, and became a Senior Lecturer, a Reader, and a Professor. He has worked on a wide variety of projects using sonic and ultrasonic methods applied to the nondestructive evaluation (NDE) and he leads the NDE Group, Imperial College London, where he is currently the Head of the Mechanical Engineering Department. He is also the Director of Guided Ultrasonics Ltd., and was the Chairman of Permasense, Ltd., Crawley, U.K., until its sale to Emerson, Inc., and also a consultant to a variety of industries. He is also a leading member of the U.K. Research Centre for NDE, Imperial College. He has authored or coauthored over 200 refereed journal articles and a similar number of conference articles in this field. He holds four current patents.